Heisenberg-Limited Frequency Estimation via Driving Through Quantum Phase Transitions

Min Zhuang,[1] Hongtao Huo,[1] Yuxiang Qiu,[1,2] Wenjie Liu,[1] Jiahao Huang ◍,[1,*] and Chaohong Lee ◍[1,2,†]

[1]*Guangdong Provincial Key Laboratory of Quantum Metrology and Sensing & School of Physics and Astronomy, Sun Yat-Sen University (Zhuhai Campus), Zhuhai 519082, China*

[2]*State Key Laboratory of Optoelectronic Materials and Technologies, Sun Yat-Sen University (Guangzhou Campus), Guangzhou 510275, China*

High-precision frequency estimation is an ubiquitous issue in fundamental physics and a critical task in spectroscopy. Here, we propose a quantum Ramsey interferometry to realize high-precision frequency estimation in a spin-1 Bose-Einstein condensate via driving the system through quantum phase transitions (QPTs). In our scheme, we combine adiabatically driving the system through QPTs with $\pi/2$ pulse to realize the initialization and recombination. Through adjusting the laser frequency under fixed evolution time, one can extract the transition frequency via the lock-in point. The lock-in point can be determined from the pattern of the population measurement. In particular, we find the measurement precision can approach the Heisenberg-limited scaling. Moreover, the scheme is robust against detection noise and nonadiabatic effect. Our proposed scheme does not require single-particle resolved detection and is within the reach of current experiment techniques, which may point out an alternative way for high-precision frequency estimation.

I. INTRODUCTION

The high-precision frequency estimation is useful for many areas ranging from fundamental physics and modern metrology science to molecular spectroscopy and global position systems [1–9]. The history of precision spectroscopy with the atomic and molecular-beam resonance method started from the 1930s, which was originally proposed by Rabi [10]. By scanning the frequency of the electromagnetic excitation around the exact resonance, a symmetric measurement signal with respect to the resonant point can be observed. The symmetric measurement signal can be used as the frequency lock-in signal to obtain the value of frequency. To improve the measurement precision, the Ramsey technique of separated oscillating field was proposed [11,12] and has been widely applied in experiments [7,13–18]. In atomic, molecular, and optical (AMO) systems, Ramsey interferometry is a generalized tool for frequency estimation. The conventional Ramsey interferometry consists of two $\pi/2$ pulses and a free-evolution process. The two $\pi/2$ pulses act as two beam splitters, and the free evolution accumulates the relative phase between the involved levels [19]. For N two-level atoms with internal states $|e\rangle$ (excited state)

and $|g\rangle$ (ground state), the transition frequency between $|g\rangle$ and $|e\rangle$ is $\omega = (E_e - E_g)/\hbar$ (we set $\hbar = 1$ in the following). In general, the interferometry starts from an initial state of all N atoms in the ground state $|g\rangle$, i.e., $|\Psi\rangle_{\text{in}} = |g\rangle^{\otimes N}$. Applying the first $\pi/2$ pulse with laser frequency ω_L slightly detuned from the atomic transition frequency ω, the input state $|\Psi\rangle_{\text{pro}} = [(|e\rangle + |g\rangle)/\sqrt{2}]^{\otimes N}$ can be prepared. Then each atom undergoes a free evolution of duration T and a second $\pi/2$ pulse is applied to recombine the two internal states. Finally, a measurement on the atomic state is performed. During evolution time T the atoms gather up a relative phase $\phi = \delta T$ with detuning $\delta = \omega - \omega_L$, which can be estimated from the measurement data. Due to the frequency ω_L and the evolution time T are known, one can recover the transition frequency ω from the relative phase ϕ. Ideally, using the product state $|\Psi\rangle_{\text{pro}}$ as input, the measurement precision can achieve the standard quantum limit (SQL), i.e., $\Delta\omega = 1/\sqrt{N}T$ [20–23], which had been realized in atomic clocks [24–26]. Quantum entanglement is a useful resource for improving the measurement precision over the SQL [27–31]. The metrologically useful many-body quantum entangled states include spin squeezed states [32–38], spin cat states [39], twin Fock (TF) state [40], Greenberger-Horne-Zeilinger (GHZ) state [41,42], and so on. Thus, a lot of endeavors had been made to generate various kinds of entangled input states. One can prepare the desired

_____

*hjiahao@mail2.sysu.edu.cn, eqjiahao@gmail.com
†lichaoh2@mail.sysu.edu.cn, chleecn@gmail.com

entangled state via dynamical evolution [27–31] or adiabatic driving [39,42–47]. For GHZ state, the measurement precision can improve to the Heisenberg limit, i.e., $\Delta\omega = 1/NT$ [27,28,41,48–56]. However, it is hard to prepare the GHZ state with large atomic number in experiments. For TF state, the measurement precision of frequency can also beat the SQL, i.e., $\Delta\omega = 1/\sqrt{N(N/2+1)}T$ [40]. Moreover, the TF state has been generated deterministically by adiabatic driving in a spin-1 atomic Bose-Einstein condensate with more than 1000 atoms [47,57–59]. However, to realize quantum-enhanced frequency estimation via entanglement, single-particle resolved detection is assumed to be necessary [19,22,40,60–67], which has been a bottleneck in practical experiments. Moreover, imperfect initial state preparation, nonideal recombination and detection are also the key obstacles that limit the improvement of measurement precision via many-body entanglement. Based on the quantum-enhanced frequency estimation via TF state, it is natural to ask the following: (i) Can one achieve Heisenberg-limited frequency measurement without single-particle resolved detection? (ii) If the Heisenberg-limited measurements are available, what are the influences of imperfection on frequency estimation in practical experiment? In this paper, we propose a scheme to implement Heisenberg-limited frequency measurement via driving through QPTs without single-particle resolved detection. Our scheme is based on a ferromagnetic spin-1 Bose-Einstein condensate under an external magnetic field. Through adjusting the laser frequency, we can extract the transition frequency ω according to the frequency lock-in signals. For every fixed frequency ω_L, one can implement quantum interferometry for frequency estimation. We combine adiabatically driving through QPTs with $\pi/2$ pulse to realize the initialization and recombination. We find that the population measurement is symmetric respect to detuning δ and reaches its maximum at the lock-in point $\omega = \omega_L$. Thus, population measurement can act as the frequency lock-in signal to obtain the value of frequency. Particularly, we find the measurement precision of the frequency can approach the Heisenberg-limited scaling.

Further, we study the robustness of our scheme against detection noise and nonadiabatic effect. We find that the detection noise and nonadiabatic effect do not induce any frequency shift on the frequency lock-in signals. For detection noise, the measurement precision of frequency $\Delta\omega$ can beat the SQL when $\sigma \leq 0.7\sqrt{N}$ in our consideration. For nonadiabatic effect, the measurement precision of frequency $\Delta\omega$ can still beat the SQL when the sweeping rate β is moderate. Compared with conventional proposal via parity measurement [40], our scheme does not require single-particle resolved detection. Our proposed scheme may open up a feasible way of measuring frequency with Heisenberg-limited scaling. The paper is organized as follows. In Sec. II, we introduce our scheme for frequency estimation. In Sec. III, within our scheme, we study two

frequency lock-in signals and frequency measurement precision in detail. In Sec. IV, we study the robustness against practical detection noise and nonadiabatic effect. In Sec. V, a brief summary is given.

II. GENERAL SCHEME

Our proposal for frequency estimation via driving through quantum phase transitions is presented below. We consider an ensemble of spin-1 atoms with three Zeeman levels: $|F = 1, m = 1\rangle$, $|F = 1, m = 0\rangle$, $|F = 1, m = -1\rangle$. Throughout this paper, we assume all time-evolution processes are unitary and abbreviate the three Zeeman levels to $|1, 1\rangle$, $|1, 0\rangle$, and $|1, -1\rangle$, respectively. Our goal is to measure the transition frequency ω between $|1, 1\rangle$ and $|1, -1\rangle$. The system states can be represented in terms of the Fock basis $|N_{-1}, N_0, N_1\rangle$. Here, $\hat{N}_m = \hat{a}_m^\dagger \hat{a}_m$ and $\hat{a}_m$ are particle number operators and annihilation operators of atoms in state $|1, m\rangle$, respectively. In our scheme, by adjusting the laser frequency ω_L, we can extract the transition frequency ω according to the frequency lock-in signals. For every fixed laser frequency ω_L, one can implement quantum interferometry for frequency estimation. The interferometry consists of four steps: (a) initialization, (b) interrogation, (c) recombination, (d) measurement, as shown in Fig. 1. In the initialization step, we consider an initial state of all N atoms in $|1, 0\rangle$ and the total atomic number N being an even integer. The evolution of the initial state $|\Psi\rangle_{\text{in}} = |0, N, 0\rangle$ is governed by the Hamiltonian:

$$\hat{H}_{\text{QPT}} = \frac{c_2}{2N}[2(\hat{a}_0^\dagger \hat{a}_0^\dagger \hat{a}_1 \hat{a}_{-1} + \hat{a}_0 \hat{a}_0 \hat{a}_1^\dagger \hat{a}_{-1}^\dagger) + (2\hat{N}_0 - 1)(N - \hat{N}_0)] - q(t)\hat{N}_0. \quad (1)$$

Here, $|c_2|(c_2 < 0)$ describes the rate of the spin-mixing process, $q = (\varepsilon_{+1} + \varepsilon_{-1})/2 - \varepsilon_0$, with ε_m being the energy of the state $|1, m\rangle$, and $q(t)$ can be tuned linearly with time in experiment. The system possesses three distinct phases through the competition between $|c_2|$ and q [47,57]. For $q \gg 2|c_2|$, the ground state is polar state with all atoms in $|1, 0\rangle$. For $q \ll -2|c_2|$, the ground state becomes TF state with atoms equally populated in $|1, -1\rangle$ and $|1, 1\rangle$. When $-2|c_2| < q < 2|c_2|$, the ground state corresponds to a superposition of all three components. The two QPT points locate at $q_c = \pm|c_2|$. In this step, we ramp $q(t)$ from $q \gg 2|c_2|$ towards $q \ll -2|c_2|$ with $q(t) = q_0 - \beta t$ to generate state $|\Psi\rangle_1 = e^{-i\int_0^{\tau_1} \hat{H}_{\text{QPT}}(t)dt}|\Psi\rangle_{\text{in}}$. Here, β denotes sweeping rate, the TF state can be adiabatically prepared when the sweeping rate is very slow. Then, a $\pi/2$ pulse with frequency ω_L act as a beam splitter to generate input state $|\Psi\rangle_2 = \hat{R}_{\pi/2}|\Psi\rangle_1$, as shown in Fig. 1(a). The frequency ω_L is slightly detuned from the atomic transition frequency ω. For simplicity, we assume the $\pi/2$ pulse is perfect. In the interrogation step, the system goes
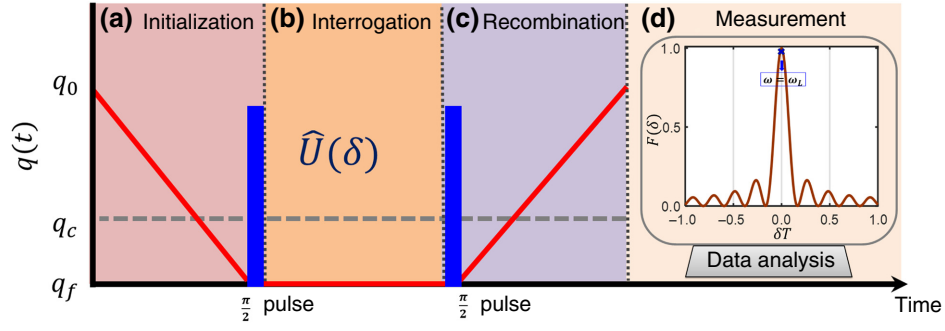
FIG. 1. Proposal of the frequency measurement scheme via driving through QPTs in the spin-1 Bose-Einstein condensate. The scheme consists of four steps: initialization, interrogation, recombination, and measurement. (a) In the initialization stage, all atoms are initially prepared in $|1, 0\rangle$. Then sweeping $q(t)$ from q_0 towards q_f very slowly to generate the TF state, and a $\pi/2$ pulse is applied on the TF state to prepare the input state. (b) In the interrogation step, the input state undergoes an interrogation stage for signal accumulation with $\phi = \delta T$. (c) In the recombination step, a second $\pi/2$ pulse is applied and then sweeping $q(t)$ from q_f towards q_0 very slowly for recombination. (d) In the measurement step, applying a suitable observable measurement on the final state. The pattern of observable measurement results versus δ can tell us the frequency lock-in point $\omega = \omega_L$. Here, $c_2 = -1$, $q_0 = -q_f = 3$, $T = 100$, and $\beta = 0.01$.

through a phase accumulation process and the output state is $|\Psi(\delta)\rangle_3 = \hat{U}(\delta) |\Psi\rangle_2$, as shown in Fig. 1(b). In the recombination step, a second $\pi/2$ pulse (using the same laser) is applied as another beam splitter to generate state $|\Psi(\delta)\rangle_4 = \hat{R}_{\pi/2}^\dagger |\Psi(\delta)\rangle_3$, and then ramping $q(t)$ from $q \ll -2|c_2|$ towards $q \gg 2|c_2|$ with $q(t) = q_f + \beta t$, as shown in Fig. 1(c). In analogy with the passive atomic clock [68–72], the two $\pi/2$ pulses also act as the local oscillator to stabilize the atomic transition frequency via measurement signals. Thus, the final state after the total sequences can be written as

$$|\Psi(\delta)\rangle_f = e^{-i\int_{\tau_1+T}^{\tau_2} \hat{H}_{\mathrm{QPT}}(t)dt} \hat{R}_{\frac{\pi}{2}}^\dagger \hat{U}(\delta) \hat{R}_{\frac{\pi}{2}}$$
$$e^{-i\int_0^{\tau_1} \hat{H}_{\mathrm{QPT}}(t)dt} |\Psi\rangle_{\mathrm{in}} . \quad (2)$$

Here, $\hat{U}(\delta) = e^{-i\delta T/2(\hat{a}_1^\dagger \hat{a}_1 - \hat{a}_{-1} \hat{a}_{-1}^\dagger)}$ describes the phase accumulation process with $\phi = \delta T$ and $\delta = \omega - \omega_L$, $\hat{R}_{\pi/2} = e^{i(\pi/4)(\hat{a}_1^\dagger \hat{a}_{-1} + \hat{a}_{-1}^\dagger \hat{a}_1)}$ is the $\pi/2$ pulse. According to Eq. (2), the final state contains the information of the estimated transition frequency ω. Ideally for $\delta = 0$, the final state $|\Psi(\delta)\rangle_f$ is identical to the initial state $|\Psi\rangle_{\mathrm{in}}$. When $\delta \neq 0$, the nonzero δ will bias the state $|\Psi(\delta)\rangle_f$ with respect to the initial state $|\Psi\rangle_{\mathrm{in}}$. In the measurement step, one can apply an observable measurement $\hat{O}$ on the final state and the expectation of $\hat{O}$ is

$$\langle \hat{O}(\delta) \rangle =_f \langle \Psi(\delta)| \hat{O} |\Psi(\delta)\rangle_f . \quad (3)$$

In the framework of frequency estimation, if the expectation $\langle \hat{O}(\delta) \rangle$ with respect to detuning δ is symmetric, the expectation $\langle \hat{O}(\delta) \rangle$ can act as frequency lock-in signal to obtain the value of frequency, as shown in Fig. 1(d). In

the next section, we introduce how to realize the high-precision frequency estimation within this framework.

III. FREQUENCY MEASUREMENT

In this section, we illustrate two frequency lock-in signals. One is the fidelity $F = |_f \langle \Psi(\delta)|\Psi\rangle_{\mathrm{in}}|^2$ between the final state $|\Psi(\delta)\rangle_f$ and the initial state $|\Psi\rangle_{\mathrm{in}}$. Another is the population measurement $\langle \hat{N}_0(\delta) \rangle$ on the state $|1, 0\rangle$. Furthermore, we find that the measurement precision of the transition frequency ω can surpass the SQL and even attain the Heisenberg-limited scaling when the particle number is large enough.

A. Frequency lock-in signals

For convenience, we assume the time-dependent evolutions both are adiabatic in our scheme. Thus, we have $|\Psi\rangle_1 = e^{-i\int_0^{\tau_1} \hat{H}_{\mathrm{QPT}}(t)dt} |\Psi\rangle_{\mathrm{in}} = |\mathrm{TF}\rangle$ and the state $|\Psi(\delta)\rangle_4$ can be written as

$$|\Psi(\delta)\rangle_4 = \hat{R}_{\pi/2}^\dagger e^{-i\delta T/2(\hat{a}_1^\dagger \hat{a}_1 - \hat{a}_{-1}^\dagger \hat{a}_{-1})} \hat{R}_{\pi/2} |\mathrm{TF}\rangle . \quad (4)$$

After some algebra, we can obtain the explicit form of the state $|\Psi(\delta)\rangle_4$ (see the Appendix for derivation). For brevity, we denote $n = N/2$ in the following. If n is even,

we have $|\Psi(\delta)\rangle_4 = |\Psi(-\delta)\rangle_4$ and it is

$$|\Psi(\delta)\rangle_4 = \sum_{m=0}^{n} A(n,m) |2n-2m, 0, 2m\rangle$$

$$+ 2 \sum_{k=0}^{n/2-1} \sum_{m_1=0}^{2k} \sum_{m_2=0}^{2n-2k} B(n,k,m_1,m_2)$$

$$\times \cos[(2k-n)\delta T]$$

$$\times |2n-2k+m_1-m_2, 0, 2k-m_1+m_2\rangle.$$
(5)

If n is odd, we have $|\Psi(\delta)\rangle_4 = -|\Psi(-\delta)\rangle_4$ and it is

$$|\Psi(\delta)\rangle_4 = 2i \sum_{k=0}^{n-1/2} \sum_{m_1=0}^{2k} \sum_{m_2=0}^{2n-2k} B(n,k,m_1,m_2)$$

$$\times \sin[(2k-n)\delta T]$$

$$\times |2n-2k+m_1-m_2, 0, 2k-m_1+m_2\rangle.$$
(6)

Here, the coefficients $A_{n,m}$ and B_{n,k,m_1,m_2} read as

$$A_{n,m} = (-1)^{n-m} \left(\frac{1}{2}\right)^{2n} \frac{C_n^{n/2}}{\sqrt{n!n!}} C_n^m \sqrt{(2m)!(2n-2m)!},$$
(7)

$$B_{n,k,m_1,m_2} = (-1)^{n-k} \left(\frac{1}{2}\right)^{2n} \sqrt{\frac{C_{2k}^k C_{2n-2k}^{n-k}}{2k(2n-2k)!}} C_{2k}^{m_1} C_{2n-2k}^{m_2}$$

$$\times \sqrt{(2n-2k-m_2+m_1)!(2k-m_1+m_2)!}.$$
(8)

The C_i^j is the combinatorial number. Furthermore, the final state is

$$|\Psi(\delta)\rangle_f = e^{-i \int_{\tau_1+T}^{\tau_2} \hat{H}_{\text{QPT}}(t)dt} |\Psi(\delta)\rangle_4.$$
(9)

When $\delta = 0$, we have

$$|\Psi(\delta=0)\rangle_f = e^{-i \int_{\tau_1+T}^{\tau_2} \hat{H}_{\text{QPT}}(t)dt} |\Psi(\delta=0)\rangle_4$$

$$= e^{-i \int_{\tau_1+T}^{\tau_2} \hat{H}_{\text{QPT}}(t)dt} |\text{TF}\rangle = |\Psi\rangle_{\text{in}}.$$
(10)

Thus, the fidelity F and the population measurement $\langle \hat{N}_0(\delta=0)\rangle$ are

$$F(\delta=0) = |_{\text{in}}\langle\Psi|\Psi\rangle_{\text{in}}|^2 = 1,$$
(11)

and

$$\langle \hat{N}_0(\delta=0)\rangle = \langle 0, N, 0| \hat{N}_0 |0, N, 0\rangle = N.$$
(12)

When $\delta \neq 0$, the final state is not exactly the initial state, thus the fidelity F and the population measurement $\hat{N}_0$ both are deviate from $F(\delta=0)$ and $\langle \hat{N}_0(\delta=0)\rangle$, respectively. According to Eqs. (5) and (6), we have $F(\delta) = F(-\delta)$ and $\langle \hat{N}_0(\delta)\rangle = \langle \hat{N}_0(-\delta)\rangle$. Thus, the fidelity F and the population measurement $\langle \hat{N}_0(\delta)\rangle$ both are δ dependent and symmetric with respect to the lock-in point $\omega = \omega_L$. Particularly, they approach their maximum when $\omega - \omega_L = 0$. It means that the fidelity $F(\delta)$ and population measurement $\langle \hat{N}_0(\delta)\rangle$ can act as the frequency lock-in signals to obtain the value of ω. In Fig. 2, the variation of fidelity $F(\delta)$ and population measurement $\langle \hat{N}_0(\delta)\rangle$ versus detuning δ are shown. The numerical results agree perfectly with our theoretical predictions. Thus, one can determine the frequency lock-in point $\omega - \omega_L = 0$ from the pattern of the two frequency lock-in signals.

B. Measurement precision

In this subsection, we illustrate the measurement precision of frequency within our scheme. Here, we characterize the measurement precision of ω via the linewidth of fidelity $F(\delta)$ and the error propagation formula with population measurement $\hat{N}_0$. First, we analyze the measurement precision via linewidth. The value of linewidth is defined as the FWHM and denoted as Γ. As shown in Fig. 2(a), it is
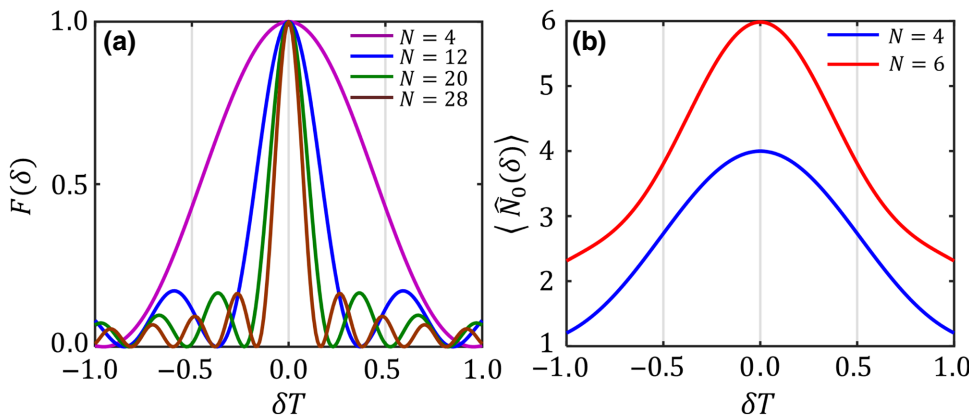

FIG. 2. The two frequency lock-in signals in our scheme. The variation of frequency lock-in signals (a) $F(\delta)$ and (b) $\langle \hat{N}_0(\delta)\rangle$ versus detuning δ for different N. They are both symmetric with respect to the lock-in point $\omega - \omega_L = 0$. Here, $c_2 = -1$, $q_0 = -q_f = 3$, $T = 100$, and $\beta = 0.01$.
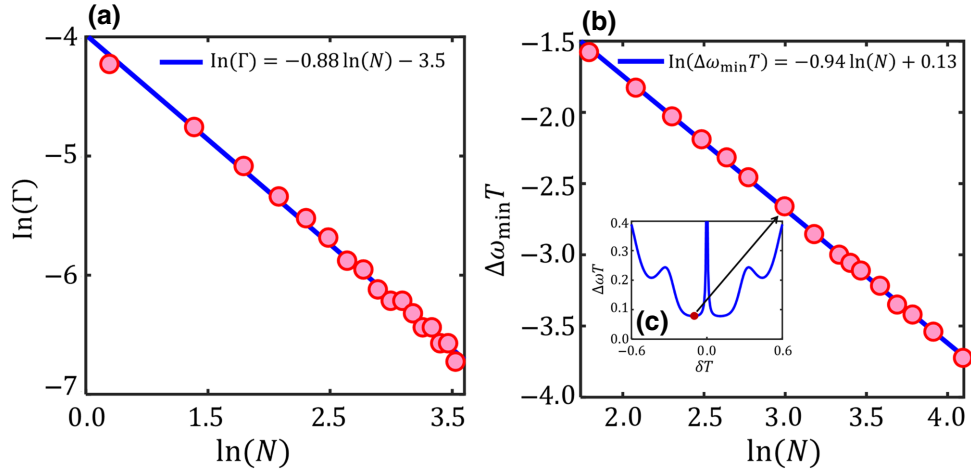
FIG. 3.   (a) Log-log scaling of the linewidth Γ versus the total particle number. The blue line is the fitting curve. (b) Log-log scaling of the optimal measurement precision $\Delta\omega_{\min}$ versus total particle number. The blue line is the fitting curve. (c) The variation of measurement precision of frequency ω versus detuning δ for $N = 20$. The black red dot corresponds to the optimal measurement precision $\Delta\omega_{\min}$, which is near the frequency lock-in point $\omega - \omega_L = 0$. Here, $c_2 = -1$, $q_0 = -q_f = 3$, $T = 100$, and $\beta = 0.01$.

evident that the linewidth $F(\delta)$ is a function of detuning δ and decreases as N increases. To confirm the dependence of Γ on the total particle number N, we numerically calculate the linewidth Γ versus N, as shown in Fig. 3(a). According to the fitting result, the log-log linewidth is $\ln(\Gamma) \approx -0.88\ln(N) - 3.5$. For N uncorrelated atoms, the log-log linewidth is $\ln(\Gamma) \approx -0.5\ln(N)$, thus our scheme can decrease the linewidth Γ effectively.

Further, we consider the measurement precision with the population measurement of $\langle \hat{N}_0(\delta) \rangle_f$. According to the error propagation formula, the measurement precision of frequency ω is

$$\Delta\omega = \frac{\Delta\hat{N}_0}{|\partial\langle\hat{N}_0(\delta)\rangle_f/\partial\omega|}. \tag{13}$$

Here, $\Delta\hat{N}_0$ is the standard deviation of $\hat{N}_0$ and can be written as

$$\Delta\hat{N}_0 = \sqrt{\langle\hat{N}_0^2(\delta)\rangle - [\langle\hat{N}_0(\delta)\rangle]^2}. \tag{14}$$

In Fig. 3(c), how the measurement precision ω changes with detuning δ is shown, and we find the optimal measurement precision $\Delta\omega_{\min}$ occurs near the frequency lock-in point $\omega - \omega_L = 0$. To confirm the dependence of $\Delta\omega$ on the total particle number N, we numerically calculate the variation of the measurement precision versus particle number, as shown in Fig. 3(b). According to the fitting result, the optimal log-log measurement precision $\Delta\omega_{\min}$ is $\ln(\Delta\omega_{\min}) \approx -0.94\ln(N) + 0.13$. It indicates that the combination of reversed adiabatic driving and population measurement is an effective way to realize quantum-enhanced frequency estimation with TF state.

IV. ROBUSTNESS AGAINST IMPERFECTIONS

In this section, we study the robustness of our scheme. In practical experiments, there are many imperfections that can influence the frequency lock-in signal and limit the final measurement precision. Here, we discuss two imperfections: the detection noise in the measurement step and the nonadiabatic effect in the initialization and recombination steps.

A. Robustness against detection noise

We study the influence of detection noise by considering the additional classical noise in the measurement process. In an ideal situation, the population measurement on the final state can be rewritten as $\langle\hat{N}_0(\delta)\rangle = \sum_{N_0} P(N_0|\delta)N_0$, where $P(N_0|\delta)$ is the ideal conditional probability, which obtains the measurement result N_0 with a given δ. However, in realistic experiment, the detection noise can limit the measurement precision of frequency. For an imperfect detector with Gaussian detection noise [31,67,68,73], the population measurement becomes

$$\langle\hat{N}_0(\delta)\rangle = \sum_{N_0} \tilde{P}(N_0|\sigma)N_0, \tag{15}$$

with

$$\tilde{P}(N_0|\sigma) = \sum_{\tilde{N}_0} A_{\tilde{N}_0} e^{-(N_0-\tilde{N}_0)^2/2\sigma^2} P(N_0|\delta). \tag{16}$$

The conditional probability depends on the detection noise σ. Here, $A_{\tilde{N}_0}$ is a normalization factor.

According to our numerical calculation, we find that the Gaussian detection noise does not induce any frequency shift on the frequency lock-in signal $\langle\hat{N}_0(\delta)\rangle$.
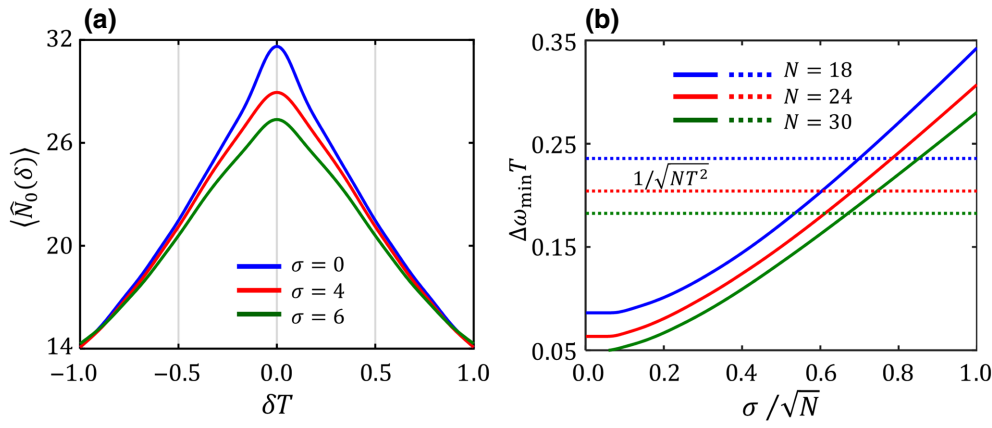
FIG. 4. The influence of detection noise on frequency estimation. (a) The variation of the frequency lock-in signal $\langle N_0(\delta) \rangle$ versus detuning δ with different detection noise σ under $N = 30$. (b) The optimal measurement precision $\Delta\omega_{min}$ versus detection noise σ for $N = 18, 24, 30$. The dotted line is the SQL, i.e., $1/(\sqrt{N}T^2)$. Here, $c_2 = -1$, $q_0 = -q_f = 3$, $T = 100$, and $\beta = 0.01$.

The frequency lock-in signal $\langle \hat{N}_0(\delta) \rangle$ is still symmetric with respect to the lock-in point $\omega = \omega_L$ and attains its maximum at the point. However, the height and the sharpness of the peak both decrease as σ increases, as shown in Fig. 4(a). To further confirm the influence of the detection noise, the optimal measurement precision $\Delta\omega_{min}$ versus the detection noise σ for different particle number N is shown in Fig. 4(b). The measurement precision can still beat the SQL when $\sigma \leq 0.7\sqrt{N}$ with

$N \in [2, 32]$. Thus our proposal is robust against to detection noise.

B. Influences of nonadiabatic effect

To realize perfect initialization and recombination in our scheme, the sweeping process should be adiabatic. However, nonadiabatic effect always exists in practical experiments. In general, the adiabaticity of the driving
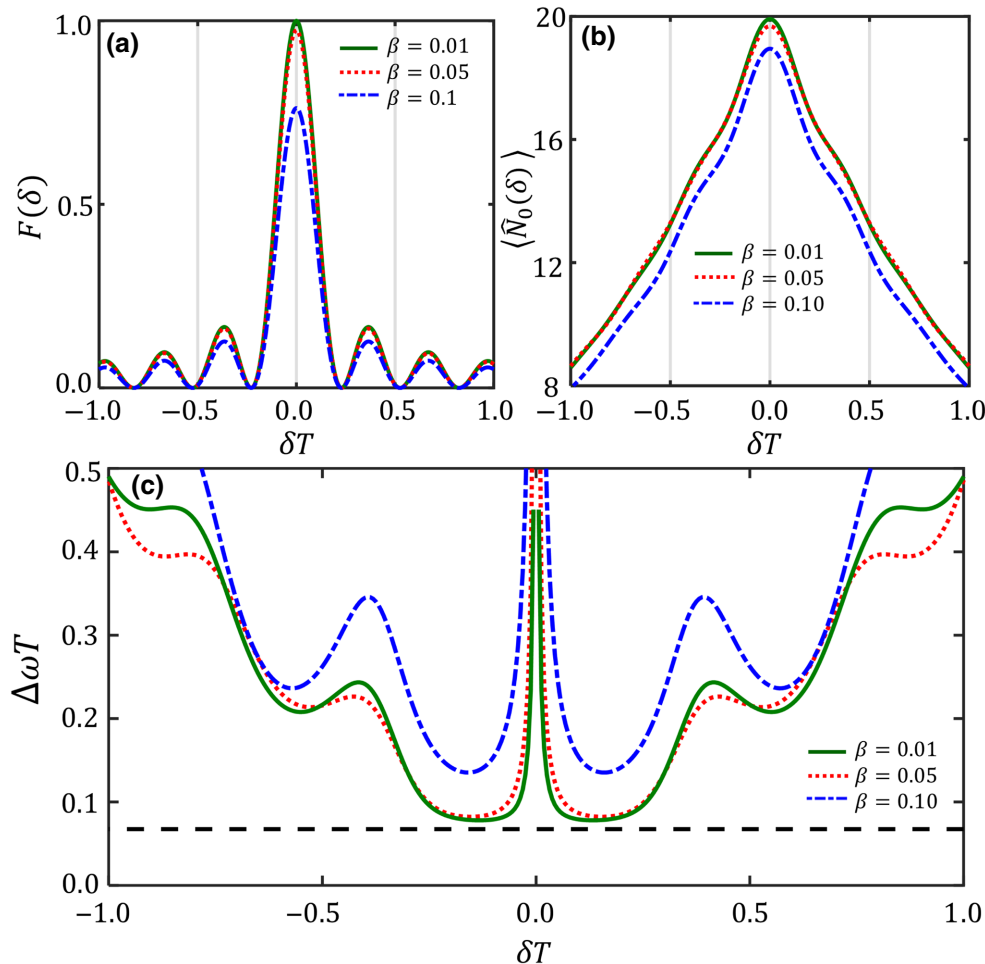

FIG. 5. Influences of nonadiabatic effect on frequency estimation. The variation of frequency lock-in signal (a) $F(\delta)$ and (b) $\langle \hat{N}_0(\delta) \rangle$ with detuning δ for different sweeping rate β under $N = 30$. (c) The measurement precision $\Delta\omega$ versus detuning δ for different sweeping rate β under $N = 20$. Here, $c_2 = -1$, $q_0 = -q_f = 3$, $T = 100$, and $\beta = 0.01$.

process can be characterized by the sweeping rate β. If the sweeping rate β is sufficiently small, the adiabatic evolution can be achieved. To confirm the influences of nonadiabatic effect on frequency estimation, the variations of the two frequency lock-in signals with different sweeping rate β are shown in Figs. 5(a) and 5(b). Our results indicate that the nonadiabatic effect also does not induce any frequency shift on the two frequency lock-in signals. The height and the sharpness of the peak also decrease as β increases. Further, we study the influence of nonadiabatic effect on the measurement precision, the variation of $\Delta\omega$ with detuning δ for different sweeping rate β is shown in Fig. 5(c). It can be observed that the measurement precision of frequency $\Delta\omega$ becomes worse as β increases, but the measurement precision of frequency $\Delta\omega$ can still beat the SQL when the sweeping rate β is moderate.

V. SUMMARY

In summary, we present a realizable scheme for performing Heisenberg-limited frequency estimation with a spin-1 Bose-Einstein condensate by driving through QPTs. In our scheme, by adjusting the laser frequency ω_L, we can extract the transition frequency ω according to the frequency lock-in signals. For every fixed laser frequency ω_L, one can implement quantum interferometry for frequency measurement. The interferometry consists of four steps: initialization, interrogation, recombination, and measurement. Particularly, we combine adiabatically driving through QPTs with $\pi/2$ pulse to realize the initialization and recombination. Based upon the proposed scheme, we find two frequency lock-in signals, fidelity $F(\delta)$ and population measurement $\langle \hat{N}_0(\delta) \rangle$, to obtain the value of ω. They are both symmetric with respect to lock-in point $\omega = \omega_L$ and achieve their maximum at the lock-in point. Further, we study the measurement precision of frequency via two different methods. We find the measurement precision $\Delta\omega$ can exhibit Heisenberg-limited scaling.

At last, we illustrate the robustness of our scheme against detection noise and nonadiabatic effect. These imperfections do not induce any frequency shift on frequency lock-in signals and just degrade the measurement precision. For detection noise, the measurement precision $\Delta\omega$ can still beat the SQL when $\sigma \leq 0.7\sqrt{N}$ in our calculation. For nonadiabatic effect, the measurement precision $\Delta\omega$ can still beat the SQL when the sweeping rate β is moderate. Compared with the conventional frequency estimation with entanglement, our proposal does not require single-particle resolution detectors and is robust against detection noise [40,41]. To realize the quantum-enhanced frequency estimation without single-particle resolution detectors in experiments, the implementation of adiabatic sweeping process is necessary. Owing to the well-developed techniques in quantum control, the TF

state can be generated by adiabatically driving a ^{87}Rb condensate undergoing spin mixing through two consecutive QPTs [47,57]. Furthermore, to extract the transition frequency ω via frequency lock-in signals, one has to adjust the laser frequency precisely. The precise implementation of $\pi/2$ pulses is a mature technology in quantum control. Thus, our scheme adds no additional complexity for the apparatus design. Our study paves an effective way to realize Heisenberg-limited frequency measurement.

APPENDIX: THE EFFECT OF $\pi/2$ PULSE ON THE GENERAL FOCK STATE

Here, we give the derivation of Eqs. (6) and (5) in the main text. The $\pi/2$-pulse operation $\hat{R}_{\pi/2} = e^{-i(\pi/4)(\hat{a}_1^\dagger \hat{a}_{-1} - \hat{a}_{-1}^\dagger \hat{a}_1)}$ just acts on $m = \pm 1$ modes. For convenience, we rewrite the $\hat{R}_{\pi/2}^\dagger$ to $\hat{U}_{\pi/2} = e^{-i(\pi/4)(\hat{a}^\dagger \hat{b} - \hat{b}^\dagger \hat{a})}$. Here, $\hat{a}$ and $\hat{b}$ are the annihilation operators for particles in mode $|a\rangle$ and mode $|b\rangle$, respectively. For a two-mode Fock state $|n_a, n_b\rangle$, we give the general derivation of $\hat{U}_\theta |n_a, n_b\rangle$ with $\hat{U}_\theta = e^{-i\theta(\hat{a}^\dagger \hat{b} - \hat{b}^\dagger \hat{a})}$,

$$
\begin{aligned}
\hat{U}_\theta |n_a, n_b\rangle &= \hat{U}_\theta \frac{(\hat{a}^\dagger)^{n_a}}{\sqrt{n_a!}} \frac{(\hat{b}^\dagger)^{n_b}}{\sqrt{n_b!}} |0\rangle_a |0\rangle_b \\
&= \hat{U}_\theta \frac{(\hat{a}^\dagger)^{n_a}}{\sqrt{n_a!}} \frac{(\hat{b}^\dagger)^{n_b}}{\sqrt{n_b!}} \hat{U}_\theta^\dagger |0\rangle_a |0\rangle_b .
\end{aligned}
\tag{A1}
$$

Due to $\hat{U}_\theta \hat{U}_\theta^\dagger = 1$, we have

$$
\hat{U}_\theta |n_a, n_b\rangle = \frac{(\hat{U}_\theta \hat{a}^\dagger \hat{U}_\theta^\dagger)^{n_a}}{\sqrt{n_a!}} \frac{(\hat{U}_\theta \hat{b}^\dagger \hat{U}_\theta^\dagger)^{n_b}}{\sqrt{n_b!}} |0\rangle_a |0\rangle_b .
\tag{A2}
$$

Then, using the basic formula: $e^{\hat{A}} \hat{B} e^{-\hat{A}} = \sum_m^\infty 1/m! [\hat{A}^{(i)}, \hat{B}]$ and the Taylor expansion, we have

$$
\hat{U}_\theta \hat{b}^\dagger \hat{U}_\theta^\dagger = \cos\theta \hat{b}^\dagger + \sin\theta \hat{a}^\dagger ,
\tag{A3}
$$

$$
\hat{U}_\theta \hat{a}^\dagger \hat{U}_\theta^\dagger = \cos\theta \hat{a}^\dagger - \sin\theta \hat{b}^\dagger .
\tag{A4}
$$

Similarly, we can obtain

$$\hat{U}_\theta \hat{b} \hat{U}_\theta^\dagger = \cos\theta \hat{b} + \sin\theta \hat{a}, \tag{A5}$$

$$\hat{U}_\theta \hat{a} \hat{U}_\theta^\dagger = \cos\theta \hat{a} - \sin\theta \hat{b}. \tag{A6}$$

When $\theta = \pi/4$, we have

$$\frac{(\hat{U}_{\pi/2} \hat{a}^\dagger \hat{U}_{\pi/2}^\dagger)^{n_a}}{\sqrt{n_a!}} \frac{(\hat{U}_{\pi/2} \hat{b}^\dagger \hat{U}_{\pi/2}^\dagger)^{n_b}}{\sqrt{n_b!}} |0\rangle_a |0\rangle_b$$

$$= \frac{\sqrt{2}(\hat{a}^\dagger - \hat{b}^\dagger)^{n_a}}{2\sqrt{n_a!}} \frac{\sqrt{2}(\hat{a}^\dagger + \hat{b}^\dagger)^{n_b}}{2\sqrt{n_b!}} |0\rangle_a |0\rangle_b. \tag{A7}$$

Particularly, when $n_a = n_b = n = N/2$, we have

$$\frac{(\hat{U}_{\pi/2} \hat{a}^\dagger \hat{U}_{\pi/2}^\dagger)^n}{\sqrt{n!}} \frac{(\hat{U}_{\pi/2} \hat{b}^\dagger \hat{U}_{\pi/2}^\dagger)^n}{\sqrt{n!}} |0\rangle_a |0\rangle_b = \frac{1}{n!2^n}(\hat{a}^\dagger \hat{a}^\dagger - \hat{b}^\dagger \hat{b}^\dagger)^n |0\rangle_a |0\rangle_b$$

$$= \sum_{k=0}^n D_n^k |2k\rangle_a |2n-2k\rangle_b. \tag{A8}$$

Here, $D_n^k = (-1)^{(n-k)}\sqrt{2k!(2n-2k)!}n!/k!(n-k)!$. Thus, Eq. (9) in the main text can be written as

$$|\Psi(\delta)\rangle = \hat{R}_{\pi/2}^\dagger e^{-i\delta T/2(\hat{a}_1^\dagger \hat{a}_1 - \hat{a}_{-1}^\dagger \hat{a}_{-1})} R_{\pi/2} |\Psi\rangle_{\text{TF}}$$

$$= e^{-i\delta(2k-n)T} \sum_{k=0}^n C_n^k \hat{R}_{\pi/2}^\dagger |2k, 0, 2n-2k\rangle$$

$$= e^{-i\delta(2k-n)T} \sum_{k=0}^n D_n^k \frac{[\hat{R}_{\pi/2}^\dagger \hat{a}_1^\dagger \hat{R}_{\pi/2}]^{2k}[\hat{R}_{\pi/2}^\dagger \hat{a}_{-1}^\dagger \hat{R}_{\pi/2}]^{2n-2k}}{\sqrt{2k!(2n-2k)!}} |0, 0, 0\rangle. \tag{A9}$$

Then, submitting Eqs. (3) and (5) into Eq. (9), we can obtain Eqs. (6) and (5) straightly in the main text. For example, for $n = 2$, the state $|\psi(\delta)\rangle$ can be written as

$$|\psi(\delta)\rangle = \left(\frac{3}{4}\cos(4\delta) + \frac{1}{4}\right)|2, 0, 2\rangle$$

$$+ i\frac{\sqrt{3}}{2\sqrt{2}}\sin(4\delta)[|1, 0, 3\rangle + |3, 0, 1\rangle]$$

$$+ \frac{\sqrt{3}}{4\sqrt{2}}[\cos(4\delta) - 1][|4, 0, 0\rangle + |0, 0, 4\rangle]. \tag{A10}$$

When $\omega = \omega_L$, we have $|\psi(\delta = 0)\rangle = |2, 0, 2\rangle$, and $F(\delta = 0) = 1$.

[1] D. Kleppner, Time too good to be true, Phys. Today **59**, 10 (2006).

[2] C. W. Chou, D. B. Hume, T. Rosenband, and D. J. Wineland, Optical clocks and relativity, Science **329**, 1630 (2010).

[3] N. Ashby and M. Weiss, *NIST Technical Note 1385* (NIST, Boulder, CO, 1999).

[4] B. J. Bloom, T. L. Nicholson, J. R. Williams, S. L. Campbell, M. Bishof, X. Zhang, W. Zhang, S. L. Bromley, and J. Ye, An optical lattice clock with accuracy and stability at the 10^18 level, Nature **506**, 71 (2014).

[5] S. Haroche, Rev. Mod. Phys. Nobel lecture: Controlling photons in a box and exploring the quantum to classical boundary. **85**, 1083 (2013).

[6] A. A. Madej, P. Dubé, Z. Zhou, J. E. Bernard, and M. Gertsvolf, ^{8}8Sr$^+$ 445-THz Single-Ion Reference at the 10^{-17} Level via Control and Cancellation of Systematic Uncertainties and Its Measurement against the SI Second, Phys. Rev. Lett. **109**, 203002 (2012).

[7] M. S. Grewal, A. P. Andrews, and C. G. Bartone, *Global Navigation Satellite Systems, Inertial Navigation, and Integration* (John Wiley Sons, New York, 2013).

[8] D. J. Wineland, Rev. Mod. Phys. Nobel lecture: Superposition, entanglement, and raising Schrödingers cat. **85**, 1103 (2013).

[9] C. W. Chou, D. B. Hume, J. C. J. Koelemeij, D. J. Wineland, and T. Rosenband, Frequency Comparison of Two High-Accuracy Al$^+$ Optical Clocks, Phys. Rev. Lett. **104**, 070802 (2010).

[10] I. I. Rabi, Space quantization in a gyrating magnetic field, Phys. Rev. **51**, 652 (1937).

[11] N. F. Ramsey, A molecular beam resonance method with separated oscillating fields, Phys. Rev. **78**, 695 (1950).

[12] N. F. Ramsey, *Molecular Beams* (Oxford, London, 1963), 124.

[13] J. L. Hall, Nobel lecture: Defining and measuring optical frequencies, Rev. Mod. Phys. **78**, 1279 (2006).

[14] T. W. Hänsch, Nobel lecture: Passion for precision, Rev. Mod. Phys. **78**, 1297 (2006).

[15] N. Hinkley, J. A. Sherman, N. B. Phillips, M. Schioppo, N. D. Lemke, K. Beloy, M. Pizzocaro, C. W. Oates, and A. D. Ludlow, An atomic clock with 10^{-18} instability, Science **341**, 1215 (2013).

[16] T. Ido and H. Katori, Recoil-Free Spectroscopy of Neutral Sr Atoms in the Lamb-Dicke Regime, Phys. Rev. Lett. **91**, 053001 (2003).

[17] T. Steinmetz, T. Wilken, C. Araujo-Hauck, R. Holzwarth, T. W. Hänsch, L. Pasquini, A. Manescau, S. Ďdorico, M. T. Murphy, T. Kentischer, W. Schmidt, and T. Udem, Laser frequency combs for astronomical observations, Science **321**, 1335 (2008).

[18] H. Margolis, Timekeepers of the future, Nat. Phys. **10**, 82 (2014).

[19] J. Huang, S. Wu, H. Zhong, and C. Lee, Quantum metrology with cold atoms, Annu. Rev. Cold At. Mol. **2**, 365 (2014).

[20] M. E. Kim, R. Sarkar, R. Fang, and S. M. Shahriar, N-atom collective-state atomic clock with $\sqrt{N}$-fold increase in effective frequency and $\sqrt{N}$-fold reduction in fringe width, Phys. Rev. A **91**, 063629 (2015).

[21] R. Sarkar, M. E. Kim, R. Fang, and S. M. Shahriar, N-atom collective-state atomic interferometer with ultrahigh Compton frequency and ultrashort de Broglie wavelength, with $\sqrt{N}$ reduction in fringe width, Phys. Rev. A **92**, 063612 (2015).

[22] D. J. Wineland, J. J. Bollinger, W. M. Itano, F. L. Moore, and D. J. Heinzen, Spin squeezing and reduced quantum noise in spectroscopy, Phys. Rev. A **46**, R6797(R) (1992).

[23] D. J. Wineland, J. J. Bollinger, W. M. Itano, and D. J. Heinzen, Squeezed atomic states and projection noise in spectroscopy, Phys. Rev. A **50**, 67 (1994).

[24] G. Santarelli, Ph. Laurent, P. Lemonde, A. Clairon, A. G. Mann, S. Chang, A. N. Luiten, and C. Salomon, Quantum Projection Noise in an Atomic Fountain: A High Stability Cesium Frequency Standard, Phys. Rev. Lett. **82**, 4619 (1999).

[25] G. Wilpers, T. Binnewies, C. Degenhardt, U. Sterr, J. Helmcke, and F. Riehle, Optical Clock with Ultracold Neutral Atoms, Phys. Rev. Lett. **89**, 230801 (2002).

[26] A. D. Ludlow, T. Zelevinsky, G. K. Campbell, S. Blatt, M. M. Boyd, M. H. G. de Miranda, M. J. Martin, J. W. Thomsen, S. M. Foreman, J. Ye, T. M. Fortier, J. E. Stalnaker, S. A. Diddams, Y. Le Coq, Z. W. Barber, N. Poli, N. D. Lemke, K. M. Beck, and C. W. Oates, Sr lattice clock at 1×10^{-16} fractional uncertainty by remote optical evaluation with a Ca clock, Science **319**, 1805 (2008).

[27] M. F. Riedel, P. Böhi, Y. Li, T. W. Hänsch, A. Sinatra, and P. Treutlein, Atom-chip-based generation of entanglement for quantum metrology, Nature **464**, 1170 (2010).

[28] B. Lücke, M. Scherer, J. Kruse, L. Pezzé, F. Deuretzbacher, P. Hyllus, O. Topic, J. Peise, W. Ertmer, J. Arlt, L. Santos, A. Smerzi, and C. Klempt, Twin matter waves for interferometry beyond the classical limit, Science **334**, 773 (2011).

[29] E. M. Bookjans, C. D. Hamley, and M. S. Chapman, Strong Quantum Spin Correlations Observed in Atomic Spin Mixing, Phys. Rev. Lett. **107**, 210406 (2011).

[30] H. Strobel, W. Muessel, D. Linnemann, T. Zibold, D. B. Hume, L. Pezzé, A. Smerzi, and M. K. Oberthaler, Fisher information and entanglement of non-Gaussian spin states, Science **345**, 424 (2014).

[31] M. Gabbrielli, L. Pezzé, and A. Smerzi, Spin-Mixing Interferometry with Bose-Einstein Condensates, Phys. Rev. Lett. **115**, 163002 (2015).

[32] M. Kitagawa and M. Ueda, Nonlinear-Interferometric Generation of Number-Phase-Correlated Fermion States, Phys. Rev. Lett. **67**, 1852 (1991).

[33] M. Kitagawa and M. Ueda, Squeezed spin states, Phys. Rev. A **47**, 5138 (1993).

[34] P. Bouyer and M. A. Kasevich, Heisenberg-limited spectroscopy with degenerate Bose-Einstein gases, Phys. Rev. A **56**, R1083(R) (1997).

[35] V. Meyer, M. A. Rowe, D. Kielpinski, C. A. Sackett, W. M. Itano, C. Monroe, and D. J. Wineland, Experimental Demonstration of Entanglement-Enhanced Rotation Angle Estimation Using Trapped Ions, Phys. Rev. Lett. **86**, 5870 (2001).

[36] A. Louchet-Chauvet, J. Appel, J. J. Renema, D. Oblak, N. Kjaergaard, and E. S. Polzik, Entanglement-assisted atomic clock beyond the projection noise limit, New J. Phys. **12**, 065032 (2010).

[37] J. G. Bohnet, B. C. Sawyer, J. W. Britton, M. L. Wall, A. M. Rey, M. Foss-Feig, and J. J. Bollinger, Quantum spin dynamics and entanglement generation with hundreds of trapped ions, Science **352**, 1297 (2016).

[38] J. Ma, X. Wang, C. P. Sun, and F. Nori, Quantum spin squeezing, Phys. Rep. **509**, 89 (2011).

[39] J. Huang, X. Qin, H. Zhong, Y. Ke, and C. Lee, Quantum metrology with spin cat states under dissipation, Sci. Rep. **5**, 17894 (2015).

[40] R. A. Campos, Christopher C. Gerry, and A. Benmoussa, Optical interferometry at the Heisenberg limit with twin Fock states and parity measurements, Phys. Rev. A **68**, 023810 (2003).

[41] J. J. Bollinger, Wayne M. Itano, D. J. Wineland, and D. J. Heinzen, Optimal frequency measurements with maximally correlated states, Phys. Rev. A **54**, R4650(R) (1996).

[42] H. Xing, A. Wang, Q. Tan, W. Zhang, and S. Yi, Heisenberg-scaled magnetometer with dipolar spin-1 condensates, Phys. Rev. A **93**, 043615 (2016).

[43] J. L. Helm, T. P. Billam, A. Rakonjac, S. L. Cornish, and S. A. Gardiner, Spin-Orbit-Coupled Interferometry with Ring-Trapped Bose-Einstein Condensates, Phys. Rev. Lett. **120**, 063201 (2018).

[44] C. Lee, Adiabatic Mach-Zehnder Interferometry on a Quantized Bose-Josephson Junction, Phys. Rev. Lett. **97**, 150402 (2006).

[45] C. Lee, Universality and Anomalous Mean-Field Breakdown of Symmetry-Breaking Transitions in a Coupled Two-Component Bose-Einstein Condensate, Phys. Rev. Lett. **102**, 070401 (2009).

[46] J. Huang, M. Zhuang, and C. Lee, Non-Gaussian precision metrology via driving through quantum phase transitions, Phys. Rev. A. **97**, 032116 (2018).

[47] Z. Zhang and L.-M. Duan, Generation of Massive Entanglement through an Adiabatic Quantum Phase Transition in a Spinor Condensate, Phys. Rev. Lett. **111**, 180401 (2013).

[48] C. A. Sackett, D. Kielpinski, B. E. King, C. Langer, V. Meyer, C. J. Myatt, M. Rowe, Q. A. Turchette, W. M. Itano, D. J. Wineland, and C. Monroe, Experimental entanglement of four particles, Nature **404**, 256 (2000).

[49] D. Leibfried, B. DeMarco, V. Meyer, D. Lucas, M. Barrett, J. Britton, W. M. Itano, B. Jelenković, C. Langer, T. Rosenband, and D. J. Wineland, Experimental demonstration of a robust, high-fidelity geometric two ion-qubit phase gate, Nature **422**, 412 (2003).

[50] D. Leibfried, M. D. Barrett, T. Schaetz, J. Britton, J. Chiaverini, W. M. Itano, J. D. Jost, C. Langer, and D. J. Wineland, Toward Heisenberg-limited spectroscopy with multiparticle entangled states, Science **304**, 1476 (2004).

[51] D. Leibfried, E. Knill, S. Seidelin, J. Britton, R. B. Blakestad, J. Chiaverini, D. B. Hume, W. M. Itano, J. D. Jost, C. Langer, R. Ozeri, R. Reichle, and D. J. Wineland, Creation of a six-atom 'Schrödinger cat' state, Nature **438**, 639 (2005).

[52] I. D. Leroux, M. H. Schleier-Smith, and V. Vuletić, Implementation of Cavity Squeezing of a Collective Atomic Spin, Phys. Rev. Lett. **104**, 073602 (2010).

[53] T. Monz, P. Schindler, J. T. Barreiro, M. Chwalla, D. Nigg, W. A. Coish, M. Harlander, W. Hänsel, M. Hennrich, and R. Blatt, 14-Qubit Entanglement: Creation and Coherence, Phys. Rev. Lett. **106**, 130506 (2011).

[54] W. Muessel, H. Strobel, D. Linnemann, T. Zibold, B. Juliá-Díaz, and M. K. Oberthaler, Twist-and-turn spin squeezing in Bose-Einstein condensates, Phys. Rev. A **92**, 023603 (2015).

[55] R. Shaniv, T. Manovitz, Y. Shapira, N. Akerman, and R. Ozeri, Toward Heisenberg-Limited Rabi Spectroscopy, Phys. Rev. Lett. **120**, 243603 (2018).

[56] C. Gross, T. Zibold, E. Nicklas, J. Estéve, and M. K. Oberthaler, Nonlinear atom interferometer surpasses classical precision limit, Nature **464**, 1165 (2010).

[57] X. Luo, Y. Zou, L. Wu, Q. Liu, M. Han, M. Tey, and L. You, Deterministic entanglement generation from driving through quantum phase transitions, Science **355**, 620 (2017).

[58] S. Guo, F. Chen, Q. Liu, M. Xue, J. Chen, J. Cao, T. Mao, M. K. Tey, and L. You, Faster State Preparation across Quantum Phase Transition Assisted by Reinforcement Learning, Phys. Rev. Lett. **126**, 060401 (2021).

[59] L. Pezzè, A. Smerzi, M. K. Oberthaler, R. Schmied, and P. Treutlein, Quantum metrology with nonclassical states of atomic ensembles, Rev. Mod. Phys. **90**, 035005 (2018).

[60] S. F. Huelga, C. Macchiavello, T. Pellizzari, A. K. Ekert, M. B. Plenio, and J. I. Cirac, Improvement of Frequency Standards with Quantum Entanglement, Phys. Rev. Lett. **79**, 3865 (1997).

[61] E. Davis, G. Bentsen, and M. Schleier-Smith, Approaching the Heisenberg Limit Without Single-Particle Detection, Phys. Rev. Lett. **116**, 053601 (2016).

[62] F. Fröwis, P. Sekatski, and W. Dür, Detecting Large Quantum Fisher Information with Finite Measurement Precision, Phys. Rev. Lett. **116**, 090801 (2016).

[63] T. Macrì, A. Smerzi, and L. Pezzè, Loschmidt echo for quantum metrology, Phys. Rev. A **94**, 010102(R) (2016).

[64] D. Linnemann, H. Strobel, W. Muessel, J. Schulz, R. J. Lewis-Swan, K. V. Kheruntsyan, and M. K. Oberthaler, Quantum-Enhanced Sensing Based on Time Reversal of Nonlinear Dynamics, Phys. Rev. Lett. **117**, 013001 (2016).

[65] O. Hosten, R. Krishnakumar, N. J. Engelsen, and M. A. Kasevich, Quantum phase magnification, Science **352**, 1552 (2016).

[66] S. S. Szigeti, R. J. Lewis-Swan, and S. A. Haine, Pumped-Up SU(1, 1) Interferometry, Phys. Rev. Lett. **118**, 150401 (2017).

[67] S. P. Nolan, S. S. Szigeti, and S. A. Haine, Optimal and Robust Quantum Metrology Using Interaction-Based Readouts, Phys. Rev. Lett. **119**, 193601 (2017).

[68] D. M. Stamper-Kurn and M. Ueda, Spinor bose gases: Symmetries, magnetism, and quantum dynamics, Rev. Mod. Phys. **85**, 1191 (2013).

[69] J. Vanier and C. Audoin, *The Quantum Physics of Atomic Frequency Standards* (Adam Higler, New York, 1992).

[70] R. Wynands, Atomic clocks, Lect. Notes Phys. **789**, 363 (2009).

[71] N. Poli, C. W. Oates, P. Gill, and G. M. Tino, Optical atomic clocks, Riv. Nuovo Cimento **36**, 555 (2013).

[72] A. D. Ludlow, M. M. Boyd, J. Ye, E. Peik, and P. O. Schmidt, Optical atomic clocks, Rev. Mod. Phys. **87**, 637 (2015).

[73] L. Pezzé and A. Smerzi, Ultrasensitive Two-Mode Interferometry with Single-Mode Number Squeezing, Phys. Rev. Lett. **110**, 163604 (2013).